ISSN 0742-0463, Journal of Volcanology and Seismology, 2023, Vol. 17, No. 4, pp. 259–277. © Pleiades Publishing, Ltd., 2023.
Russian Text © The Author(s), 2023, published in Vulkanologiya i Seismologiya, 2023, No. 4, pp. 3–22.

The 2022 Activity of Ebeko Volcano: The Mechanism and Ejecta

T. A. Kotenko[a], *, S. Z. Smirnov[b, c], **, and T. Yu. Timina[b], ***

[a] *Institute of Volcanology and Seismology, Far East Branch, Russian Academy of Sciences, Petropavlovsk-Kamchatsky, 683006 Russia*

[b] *Sobolev Institute of Geology and Mineralogy, Siberian Branch, Russian Academy of Sciences, Novosibirsk, 630090 Russia*

[c] *Trofimuk Institute of Petroleum Geology and Mineralogy, Siberian Branch, Russian Academy of Sciences, Novosibirsk, 630090 Russia*

**e-mail: sinarka2017@mail.ru*

***e-mail: ssmr@igm.nsc.ru*

****e-mail: timina@igm.nsc.ru*

Received January 31, 2023; revised March 27, 2023; accepted April 10, 2023

Abstract—This paper provides information on the 2022 eruptive activity of Ebeko Volcano. Phreatic explosions had been occurring in the crater lake from January 22 to June 13 due to water seepage through a plug in the upper part of the magma conduit with subsequent boiling. Vulcanian type explosions started since June 14 and dried the lake. The ash particle-size distribution changed toward smaller sizes. Petrographic, mineralogical, and geochemical studies of the tephra define this period as a phreatomagmatic eruption based on the presence of fresh juvenile material. Interaction between magma and waters of the Ebeko hydrothermal system results in its depletion in alkali and enrichment in silica. We hypothesize that the formation of amorphous water-bearing silica in the form of numerous segregations and its subsequent dehydration can favor the volcano's explosive activity.

Keywords: Ebeko Volcano, Ebeko, crater lake, phreatic, phreatomagmatic

DOI: 10.1134/S0742046323700264

INTRODUCTION

Ebeko is an active volcano in the northern part of Vernadsky Range on Paramushir Island, Kuril Islands, Russia (Fig. 1a). It is also one of the active volcanoes on the Kuril Islands with summit crater lakes. Among the active stratovolcanoes and edifices in the systems of volcanic ranges of the Kuril Islands, summit lakes recently exist in the craters of Raikoke Volcano on Raikoke Island and Pallas Volcano on Ketoi Island (Kozlov, 2015; Melnikov et al., 2020). The other crater lakes are confined to larger caldera complexes on Onekotan (Koltsevoe and Chernoe), Simushir (Biryuzovoe), and Kunashir Island (Kipyashchee and Goryachee) (Gorshkov, 1967; Kozlov, 2015). The lakes play an important role, governing the eruptive styles, because they favor the formation of fissure and pore waters in cooling magma bodies. The heating of these waters by magma, as well as direct contact with magma, produce explosive eruptions. The presence of a lake in the crater of an active volcano is a source of hydrologic hazards, e.g. lahar generation (Kilgour et al., 2010; Mastin and Witter, 2000; Rouwet et al., 2014).

Following the widely used terminology (Barberi et al., 1992; Christenson et al., 2010; Németh and Kósik, 2020; Pardo et al., 2014; Stix and de Moor, 2018) phreatic eruptions are those, in which: 1) magma is just a source of thermal energy and is not directly involved in eruptions, volcanic ejecta contains scarce if any juvenile material; 2) steam and other gases of primarily meteoric origin expanding in pores and cracks of volcanic rocks are a primary driving force for the eruption. According to (Barberi et al., 1992; Christenson et al., 2010), a phreatic eruption should be defined as explosive destruction of the gas-resistant plug of solidified magma in the vent.

Phreatomagmatic eruptions combine the characteristics of magmatic and phreatic eruptions, since they are caused by exogenous waters encountering the magma (Zimanowski et al., 2015). The phreatomagmatic ejecta must necessarily contain a juvenile material (Alvarado et al., 2016; Zimanowski et al., 2015). These authors reduce the phreatomagmatic explosion mechanism to the extensive vapor expansion when magma directly contact with surface waters, e.g., on the bottom of crater lakes, when emplaced into aquifers or when coming in contact with the edifice rocks that contain pore and fissure waters of hydrothermal systems. This leads to fragmentation of the magma and the country rock of the edifice (Houghton et al., 2015;

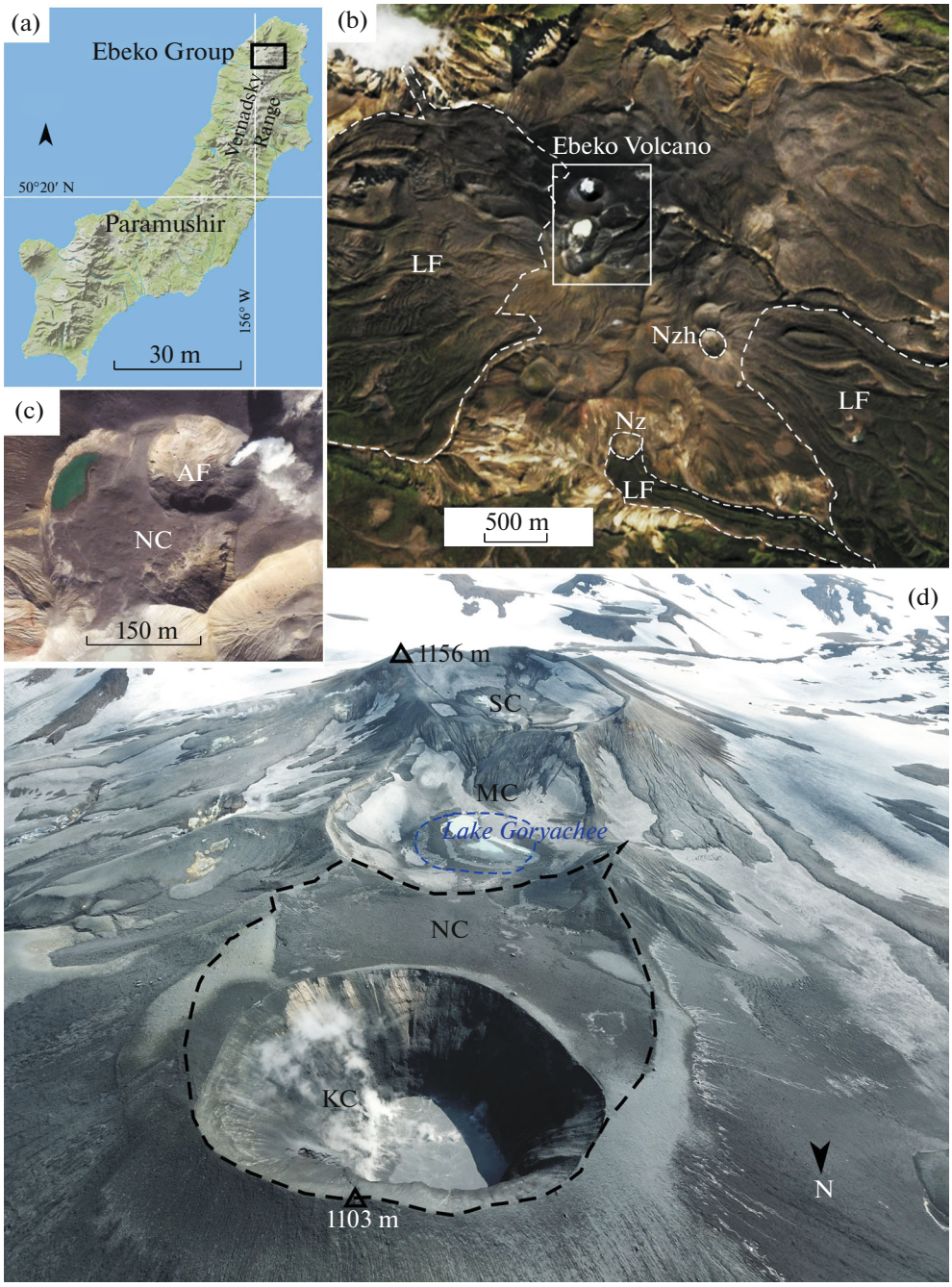

Fig. 1. The geographic location of the objects of study. (a) Volcanoes in the Ebeko group, Paramushir Island; (b) volcanoes of the Ebeko group (Nz Nezametnyi, Nzh Neozhidannyi, LF lava flows); (c) Northern Crater (NC) with an inner crater, Active Funnel (AF) in 2012; (d) aerial photograph of Ebeko Volcano, June 6, 2022 (KC—Korbut Crater, NC—Northern Crater, MC—Middle Crater, SC—Southern Crater). Photographed by M.L. Kotenko.

Morrisey et al., 1999; Wohletz, 1983). Intermittent phreatomagmatic explosions can last between a few months to a few years with varying frequency and vigor.

The understanding of the nature and relationships between phreatic and phreatomagmatic eruptions occurring simultaneously in the same eruption center provides valuable information on the interaction of the plumbing system of the active volcano with the surface and underground waters, thus enabling researchers to assess the dynamics of long periods of activity and to predict volcanic hazard. The present study provides new data on the ongoing period of activity at Ebeko volcano that started in 2016; a quiescent period occurred in the fall of 2021 and the early winter of 2022. It changed to a new period of activity, exhibiting

features of phreatic and phreatomagmatic eruptions, in late January.

THE GEOLOGICAL STRUCTURE AND VOLCANIC ACTIVITY OF VOLCANOES IN THE EBEKO GROUP

Ebeko Volcano is part of the complex volcanic massif located on Vernadsky Range (Paramushir Island). The basement of this massif is composed of Miocene and Miocene-Pliocene volcanogenic and volcano-sedimentary rocks (*Noveishii ...,* 2005) with fragmented remains of Late Pliocene to Early Holocene lava plateaus and extinct volcanoes in the northern part of the range (Melekestsev et al., 1993b; *Opyt ...,* 1966). Extinct cones of other volcanic edifices, which were formed almost simultaneously with Ebeko, are distributed in vicinity of the major Ebeco edifice (Fig. 1b). This group of volcanic edifices is commonly referred to as the Ebeko group (*Noveishii ...,* 2005). These edifices are strongly damaged by tectonic processes and erosion. The edifices of the Holocene Ebeko and Neozhidanny volcanoes are composed mostly of pyroclastic material. However, extensive lava fields (~5 and ~9 km^2, respectively) are located at the foots of these volcanoes (Gorshkov, 1967; Melekestsev et al., 1993a). The monogenic Nezametny Volcano does not have a well-pronounced cone. The narrow lava flow was discharged through the southeastern rim of a small crater. Compositions of lavas ejected by the Ebeko group volcanoes vary from basalts to andesites (Panin et al., 2015). According to Melekestsev et al. (1993a), the eruptions of Neozhidanny and Nezametny occurred not later than 2.4–3 Ka ago, while Ebeko Volcano persists in activity until the present time.

According to Gorshkov (1967), Ebeko Volcano is a complex nested edifice. It consists of three coalesced cones containing large craters (Yuzhny (Southern), Sredny (Middle), and Severny (Northern) craters) making an elongated from south to north linear group. The cones are based on a lava plateau composed of flows that went down the western slope of the Vernadsky range into the valleys of the Gorshkov and Yuriev rivers.

Ebeko Volcano hosts a hydrothermal system (Belousov et al., 2002; Kalacheva et al., 2015) with powerfull external manifestations on the outer slopes of the cones and inside the craters (fumaroles, hot springs, boiling water-mud basins). As well, ultra-acid thermal lakes arise periodically within the craters.

The historical eruptions at Ebeko, the most complete review of which can be found in (Gorshkov, 1967; Gushchenko, 1974; Melekestsev et al., 1993a, 1993b; Belousov et al., 2021), occurred in 1793, 1859, 1934–1935, 1963, 1965, 1967–1971, 1987–1991, 2009, 2010, 2011, and in 2016–2021. All of them were purely explosive. Vents have been opened mostly within craters of the Middle and Northern cones. Only two new vents, i.e. 1963 vent in the Vostochnyi Tsirk (Kirsanov et al., 1964) and 2005 vent on the eastern slope of Lagernyi Creek (Kotenko et al., 2010), appeared outside of these craters. Some eruptions occurred (or started occurring) in crater lakes (Basharina and Khramova, 1971; Kotenko et al., 2010, 2012; Melekestsev et al., 1993b; Skripko et al., 1966): in 1965, 2011 explosions occurred through the lake Goryachee of Middle Crater; and in 1967, 1989, and 2006–2007 through the lakes within Northern Crater.

Since 1989 Northern Crater showed the highest activity. The present-day center of volcanic activity began to form in 2018 and was named Korbut Crater (KC) (see Fig. 1d) (Kotenko et al., 2019) or New-North-Crater in English-language literature (Walter et al., 2020); it is confined to the northern rim of Northern Crater. Pyroclastic material that was ejected from KC completely buried the previous crater (Active Funnel, see Fig. 1) (Kotenko et al., 2019; Belousov et al., 2021). A new lake appeared in KC in late 2021 (Kotenko, 2022).

THE DATA SET AND THE METHODS OF STUDY

Field observations and photographing in the zone around the crater were used as visual tools of eruption activity monitoring. The remote monitoring techniques included continuous frame-by-frame photographing at 5 s rate with unmanned Brinno TLC 100 camera, installed at 7 km from the volcano; aerial photosurveys using a MAVIC Pro Platinum UAV equipped with a 12-megapixel digital camera; and analysis of the European Space Agency (ESA) satellite images (https://apps.sentinel-hub.com/eo-browser). Data on thermal anomalies provided by the MIROVA project (https://www.mirovaweb.it/?action=volcanoDetails_S2&volcano_id=290380).

The temperature at the lake surface was measured using an infrared Kelvin compact 1200 thermometer with accuracy ±1°C. The linear dimensions of the lake were determined using a GLM 250 VF laser distance meter manufactured by BOSCH (Germany). The area of lake surface in the KC was measured based on the aerial surveying data and estimated using images from the ESA Sentinel 2 satellite (https://apps.sentinel-hub.com/eo-browser). For the KC closed drainless basin having the shape of a truncated cone the lake surface area (LSA) was chosen as a best monitoring tool out of three possible morphometric characteristics (lake surface area, water level and volume). The daily total precipitation were obtained from data for the nearest weather station of Rosgidromet Agency #32215, located in Severo-Kurilsk city at 23 m a.s.l. and 7 km apart from Ebeko Volcano.

The chemical composition of water sampled from the KC lake was determined at the Laboratory of Post-

magmatic Processes, Institute of Volcanology and Seismology, Far East Branch, Russian Academy of Sciences (IVS FEB RAS).

The steam-gas emission from the KC was determined by two methods. The first one is based on the plume height with account for a wind speed in the plume layer (Fedotov, 1982), while the other uses comparison of plume projection areas onto UAV-borne photographic survey plane (Hochstein and Bromley, 2001). The gas discharges for the thermal fields that were accessible in a winter time (those on the Yugo-Vostochnyi (South-Eastern) and Southern craters) were obtained by direct measuring gas-flow velocity at the fumarole mouth using a Pitot tube, gas temperature using an IT-8 digital thermometer with a Chromel-Alumel thermocouple, and the diameter of the gas channel (Nekhoroshev, 1960).

Fresh ash and bombs were sampled at the rim of the Korbut Crater and within 1 km distance from it. Some samples of volcanic ash were taken just after a explosions from the clothing and from the surface of the backpacks of the authors of this study.

For morphological and micro analytical studies the ash samples from the 2022 explosions were ultrasonically cleaned from the ultra-fine fraction (<50 μm). The morphological and microanalytical studies of the ash particles were performed using a TESCAN MIRA 3 LMU scanning electron microscope (at the Center for Multielement and Isotopic Studies of the Institute of Geology and Mineralogy SB RAS, Novosibirsk) equipped with a field-emission source of electrons and an X-Max 50 energy dispersive (EDS) X-ray detector manufactured by Oxford Instruments (Great Britain). The EDS microprobe analysis was performed at an accelerating voltage of 20 kV. The probe current was 1 nA and size – 10 nm. The spectrum accumulation time during the analysis of minerals and glass in ash particles was 60 seconds. To avoid underestimating Na in glass the survey was performed by scanning an area whose size was chosen to be at least 5 × 5 μm. Composition of the spot was determined by averaging the results for 2–3 nearby located areas. The instrument was calibrated using well-characterized intralaboratory standards. Compositions of clinopyroxene and plagioclase phenocrysts, whose stoichiometry implies a 100% total for a full microprobe analysis, have been periodically measured in vicinity of the glass analysis spots in order to check for accuracy and monitor the drift of conditions. When the total of phenocryst analysis was outside the range 99–101 wt %, the concentrations of all elements in glass were multiplied by a constant obtained from division of 100 to the phenocryst analysis total.

In order to assess a particle-size distribution an ash sample was divided into fractions >1 mm and <1 mm. Weight percentage for each fraction was determined. The size distribution for the <1 mm fraction was measured using an Analysette 22 Laser Particle Sizer instrument (Fritsch, Germany) at the Laboratory of Cenozoic Geology IGM SB RAS. The results of the analysis were presented in volume fraction percentages.

The major-element compositions of ashes and bombs were determined by X-ray fluorescence using an ARL 9900XL spectrometer (Thermo Fisher Scientific, USA) at the Center of Multielement and Isotopic Studies at IGM SB RAS. The loss on ignition (LOI) was determined after holding the sample for 2 hours at 950°C.

THE RESULTS OF OBSERVING THE ACTIVITY IN THE KORBUT CRATER AND THE DYNAMICS OF SIZE CHANGES FOR THE CRATER LAKE

The State of the Korbut Crater from November 20, 2021 to January 21, 2022

The period of preceding activity involved frequent Vulcanian type explosions, and lasted from October 19, 2016 to November 19, 2021 (http://geoportal.kscnet.ru/volcanoes/volc?name=Ebeko). Relatively powerful, but infrequent explosions occurring at the end of that period (August to November 2021) probably showed a decelerating ascent or even a complete stall of magma, or else arrival of strongly degassed magma portions. This was a reason why the next explosion required a longer period of quiescence. The pause between large events may have lasted for 14–26 days. At the same time, the concentration of SO_2 in the eruption gases since the mid-August decreased by a factor of two in comparison with the previous year (Kotenko et al., 2022). This might be an evidence of the depletion of gas phase in magmatic components.

This stage was followed by a quiescence from November 20, 2021 to January 22, 2022, with high fumarolic activity persisting in the KC. Fumaroles were active on the bottom and at the inner walls of the crater. The crater dimensions along the rim were 230 m and 205 m, and the measured depth was ~100 m. We estimate that the amount of steam and gas emission from the KC in November to early December 2021 was ~1350 t/day. When combined with atmospheric precipitation, this created conditions for the appearance of a new crater lake. The lake had an area of 4500 m^2 by January 12, 2022 with the water temperature at the surface being 43°C (Kotenko and Kotenko, 2022). Underwater fumarolic discharge occurred in the form of convective cells that could be seen on water surface. Fumaroles were also active above water level at the western and northern crater walls.

The Activity in the Korbut Crater January 22–June 13, 2022

Until January 22, 2022, the monitoring facilities did not reveal any explosions from the Korbut Crater.

The exact date when the new eruption started is difficult to determine because of limitations that restricted the visual and instrumental monitoring of the volcano summit during a wintertime. The limitations stem mainly from unfavorable weather conditions: low clouds and snowstorms did not allowed observation and photographing of the volcano from the ground or from space. In addition, the short daylight duration limited photographing time even under favorable weather conditions. The first samples of fresh ash were taken on January 22, 2022 southeast of the volcano with an observed northwest wind at the level of crater rim. The ashfall was observed in the town of Severo-Kurilsk 7 km from the volcano on January 24 at 2:40 UTC, with the wind coming from west. The volcano was not visible at the time of ashfall. On February 2 at 0:08 UTC we succeeded in direct observation of an explosive ejection from the Korbut Crater. A similar explosion was recorded by photo and video survey on February 5 (Fig. 2a, 2b, 2c). The photographs show that fan of ash-steam-gas 'cock's tail' jets (nomenclature after Thorarinsson et al., 1964) forms at the early phase of explosion. At the initial instant of the discharge, steam and tephra jets went in different directions and speeds (but not over 60 m/s). The greatest height, which the tephra reach was not higher than 600 m above the crater. Much of mostly coarsely grained material fell back into the crater due to gravitational separation of the erupted mixture, while the steam and gas clouds rose up to 0.5–2.5 km and were dispersed there during a few minutes after the discharge.

Similar explosions, but with a lower ash load, had been observed until June 13. Lifetime of steam and gas plumes and clouds of these explosions did not exceed a few minutes. After an explosion, color of water mixed with clastic material in the new crater lake stayed black for 20–30 min more (Fig. 3). The mixture of clastic material and water discharged beyond the crater rim was deposited on the outer snow-laden slopes of the crater; producing wet blankets (see Fig. 3). Numerous shallow channels up to 15 cm deep cut the snow cover under the bottom of such blanket on April 5 after the explosion at 22:49 UTC. A similar character of eruption deposits on a snow-covered volcanic cone was described, e.g., in 2002 and 2004 during eruptions from the lake in the southern crater of Korovin Volcano, Aleutian Islands, USA (Waythomas, 2022).

The Change in Size of the Lake in the Korbut Crater

The lake surface area (LSA) in the Korbut Crater has been measured periodically since December 11, 2021. The LSA dynamics diagram (Fig. 4) demonstrates that the smallest LSA was recorded on February 13, and after that has been increasing until the end of May. Direct snowfalls, as well as snowdrifts carrying snows from other areas of the Northern Crater into the Korbut Crater, were a major source for recharge of the lake with meteoric waters before the May, 10. The precipitations in May were insignificant (see Fig. 4), but intense snow melting started at the crater levels. Based on aerological sounding data (https://weather.uwyo.edu/cgi-bin/sounding), the mean height of the zero isotherm has been 1820 m or higher since May, 7. This means that mostly positive air temperatures were observed at the crater level. The greatest LSA of 9400 m^2 was recorded in May 27–30, after which it became decreasing. The dynamics of LSA variations in the KC is represented in Fig. 5. The photo of the lake was taken on April 6, before the explosion (see Fig. 5a), and 17 min after the explosion (see Fig. 5b): the water changed its color from milky blue to black, demonstrating the encountering of abundant suspension (pyroclastic material) in the lake water. The inner walls of the crater were completely covered by a mud. On June 6 and 12 (see Figs. 5c, 5e) the lake in the Korbut Crater was divided into two parts. The deeper northern part (about 30% of lake area) with underwater fumarolic discharge and a shallow southern part with fumarolic jets forcing their way through the bottom deposits where the fumaroles emitted sucking sounds while periodically penetrating through the viscous sediment mass overflowing their mouths. On June 24 we observed just a small oval lake in the northeastern part of the bottom surrounded by terraced pyroclastic sediments from the south and west. The lake in the KC disappeared after June 24. A dry crater was observed on July 18 and September 18 (see Figs. 5d, 5f) with vigorous discharge of steam and gas in the deeper northeastern part, while terraces of ash deposits towered above it from the south and west.

We tried twice to sample the lake water in order to determine its chemical composition. However, the attempts have failed, and we analyzed water from ice lenses, which were formed by lake waters ejected from the crater by the February 5 and 20 explosions. For this water the following values have been determined: pH ~ 2.7, the concentration (g/L) of sulfate ions 3.4 and 1.7, of chlorine ions 3.3 and 0.4, the molar SO_4/Cl ratios were 0.4 and 1.5, respectively. The resulting characteristics indicate that the KC contained an ultra-acid sulfate-chloride lake.

The Activity in the Korbut Crater Since June 14, 2022 Until the Present

Beginning on June 14, the character of the explosions, the volume of ejected ash material, the shape and height of pyroclastic plumes, all changed sharply. The earlier explosions produced "cauliflower" type black colored ash plumes, which also, similarly to February–June 2022 explosions, were gravity separated into solid material and steam and gas mixture, giving snow-white caps of steam on top of the black column. The later explosions formed plumes with larger volumes showing faster ascent rates. The plumes became dark grey, and the steam caps were observed only during the terminal phase of the discharge.

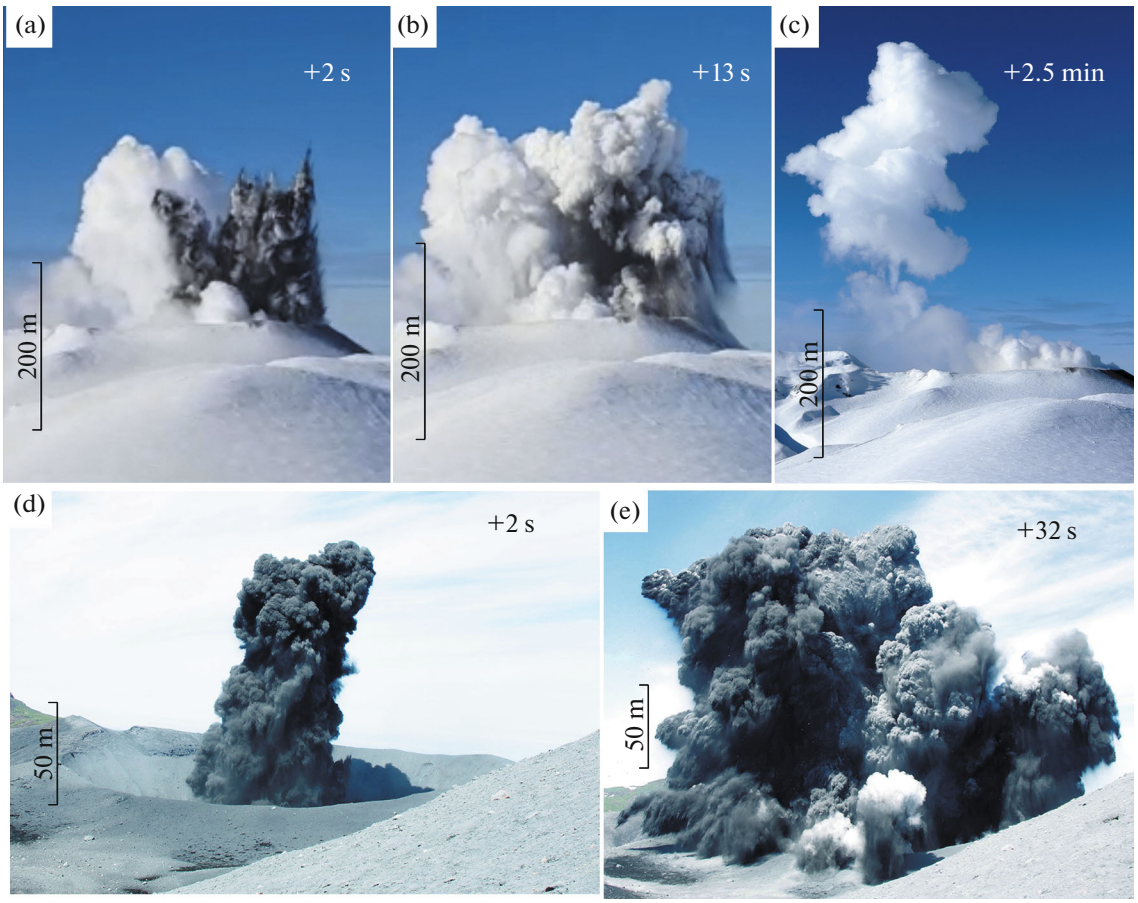

Fig. 2. Phreatic explosions at 23:41 UTC, February 5 (a–c) and at 3:10 UTC, June 24 (d, e). The times at the photos are measured from the start of the explosion. Inner steam jets and steam caps on the heads of ash jets are prominent in Fig. 2e, which is typical of phreatomagmatic explosions. Photographed by E.I. Kotenko (a–c) and by T.A. Kotenko (d, e).

Observation of individual discharges showed that relatively thin oblique jets were formed at their initial phases, and only after that, a massive ash cloud began to form gradually transforming into a thick vertical plume. Such plumes could reach heights up to 4 km a.s.l. Base surges were formed in the course of especially powerful explosions. The discharges of the reported period show features of Vulcanian type of eruptions.

The frequency of explosions have increased since June 11. As an example, on June 24 discharges were observed every 1.5 hours on average (see Figs. 2d, 2e), the ash plumes rose up to 0.4–3.4 km above the crater, and the ash plume trails extended over 15 km long. On July 8, the pause between explosions diminished to 58 min on average, varying between 2 min and 3.5 h. On some days, e.g., July 3 and 8, thick posteruptive gas trails persisted for 30-50 min after the explosions carrying small admixtures of ash and extending for 10–12 km. These trails were similar to gas trails produced by the explosions in 2020–2021 (Kotenko et al., 2022). The initial velocities of ash-loaded gas jets during the 2022 eruptions estimated on the basis of photo and video surveys were commonly 20–60 m/s, reaching 130–150 m/s during very strong explosions hurling large bombs to distances up to 0.8 km from the vent.

Since June 11 MIROVA (https://www.mirovaweb.it) and KVERT (http://www.kscnet.ru/ivs/kvert/van/index?type=3) also began to provide reliable records of thermal anomalies in the Korbut Crater.

A DESCRIPTION OF THE EJECTA

The material ejected by the first explosions in the Korbut Crater was a mixture of lake water with suspended pyroclastics. After June 14 (the second period), tephra that fell near the crater (0–800 m) frequently came as ash-laden rains or as slow ash settling. The bands of the falling ejecta look like a multitude of curved vertical thin trickles. Volcanic bombs and ballistic blocks, the most distal of which occasionally were as large as 40 cm across, in middle of August began to fall in the proximal zone of the crater within 0.8 km. First bombs of the ‘breadcrust’ type were ejected to a distance of 50 m from the crater rim on August 19.

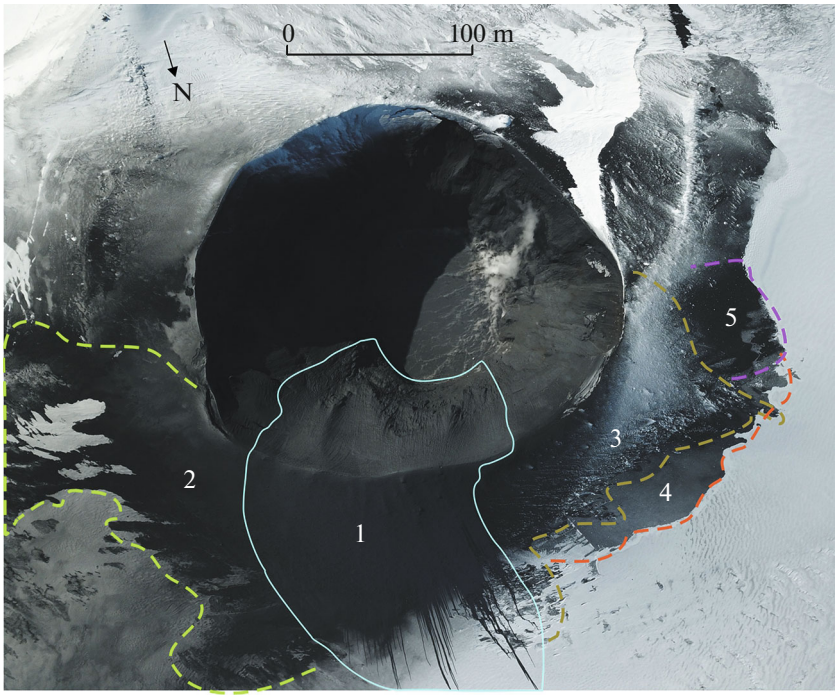

Fig. 3. Blankets and flows of water-charged pyroclastic mixture ("mud") ejected from the new lake in the KC and deposited on the slopes of the Korbut Crater: fresh flows were discharged on April 5, 2022 after the explosion at 22:49 UTC (1) and others after preceding explosions (2–5). Aerial photograph by M.L. Kotenko.

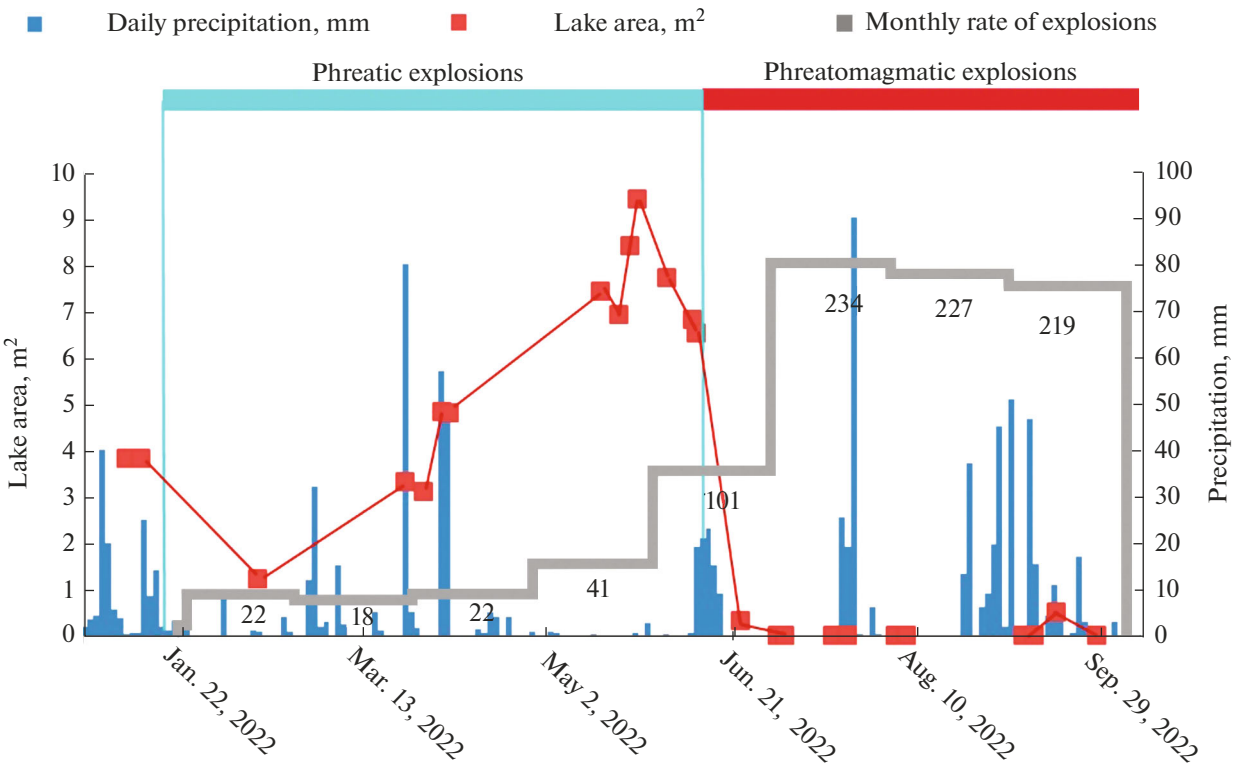

Fig. 4. A diagram showing the variation in lake area in the Korbut Crater, total daily precipitation (for height 23 m b.s.l., the nearest weather station is Severo-Kurilsk #32215), and the number of recorded explosions per month from the Korbut Crater with indication of periods of inferred phreatic and phreatomagmatic activity.

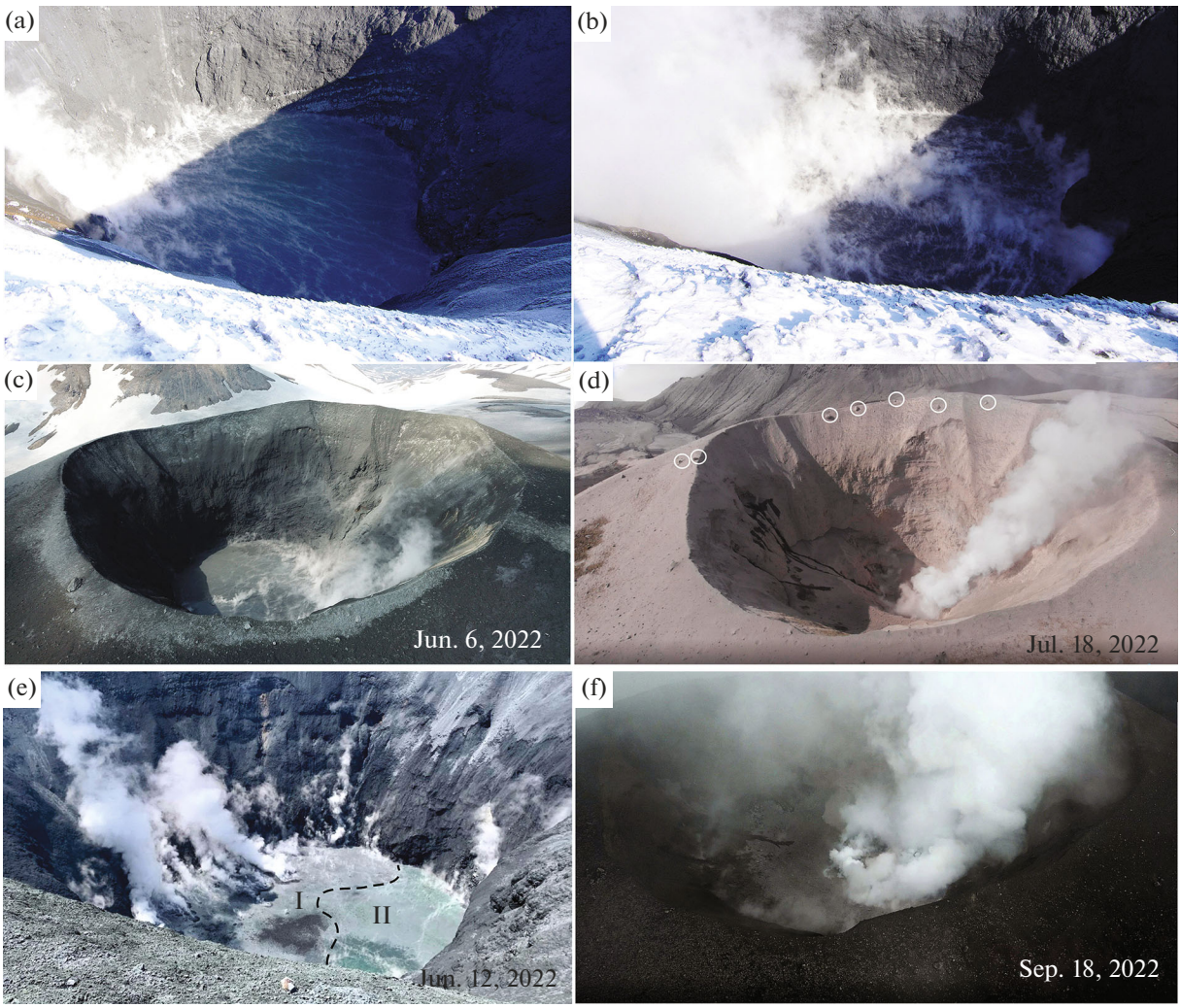

Fig. 5. The variation in KC lake area. (a, b) Lake in Korbut Crater at 9:26 UTC, April 6 before explosion (LT = UTC + 11h) (a) and at 9:43 LT after explosion (b); (c, d) Korbut Crater on June 6 with a lake (c) and on July 18 without a lake (d), view from south (white circles at crater rim on July 18 mark large fresh 'breadcrust' bombs); (e) lake on June 12 (dashed line separates the shallow area (I) and a deeper area (II) with underwater fumarolic discharge on the north side, view from northeast; (f) Korbut Crater on September 18 (vigorous fumarolic activity is concentrated in the northeastern part of the bottom). Aerial photographs made by M.L. Kotenko (c, f) and by K.A. Petrov (d). Photographed by T.A. Kotenko (a, b) and by D.A. Ermolaev (e).

Ash Particle-Size Distribution and Morphology

Figure 6a shows the mass fractions of the fine and the coarse fraction in the samples of solid material discharged by the explosions. The balance between the different fractions clearly distinguishes two periods, from January to June (the first period) and from June to September (the second period) of 2022. It is clear in this figure that significant amount of the >1 mm fraction, which varies between 66 and 17 wt %, is typical of the first period, while in the solid material discharged during the second period this fraction comprises less than 6 wt %.

The particle-size distribution (PSD) of the finer (ashy) fractions in the solid material also differs between the two periods. The PSD in the ashes discharged during the first period demonstrates three modes: between 5 and 20 μm with a maximum at 10–15 μm, between 50 and 90 μm with a maximum at 50–70 μm, and between 100 and 500 μm with a maximum at 250–400 μm (see Fig. 6b). The particles with sizes between 100 and 500 μm dominate over others. The ashes discharged during the second period also demonstrate three modes in the same size ranges, but with a greater percentage for the 50–90 μm fraction whose maximum is displaced toward 50–60 μm. The greatest number of particles with size 100–500 μm in the ashes discharged during the second period occurs in the range 100–200 μm, while the percentage of the larger particles nearly vanishes (see Fig. 6c).

Scanning electron microscopy (SEM) using the method of back scattered electrons (BSE) revealed that the overwhelming number of juvenile particles in

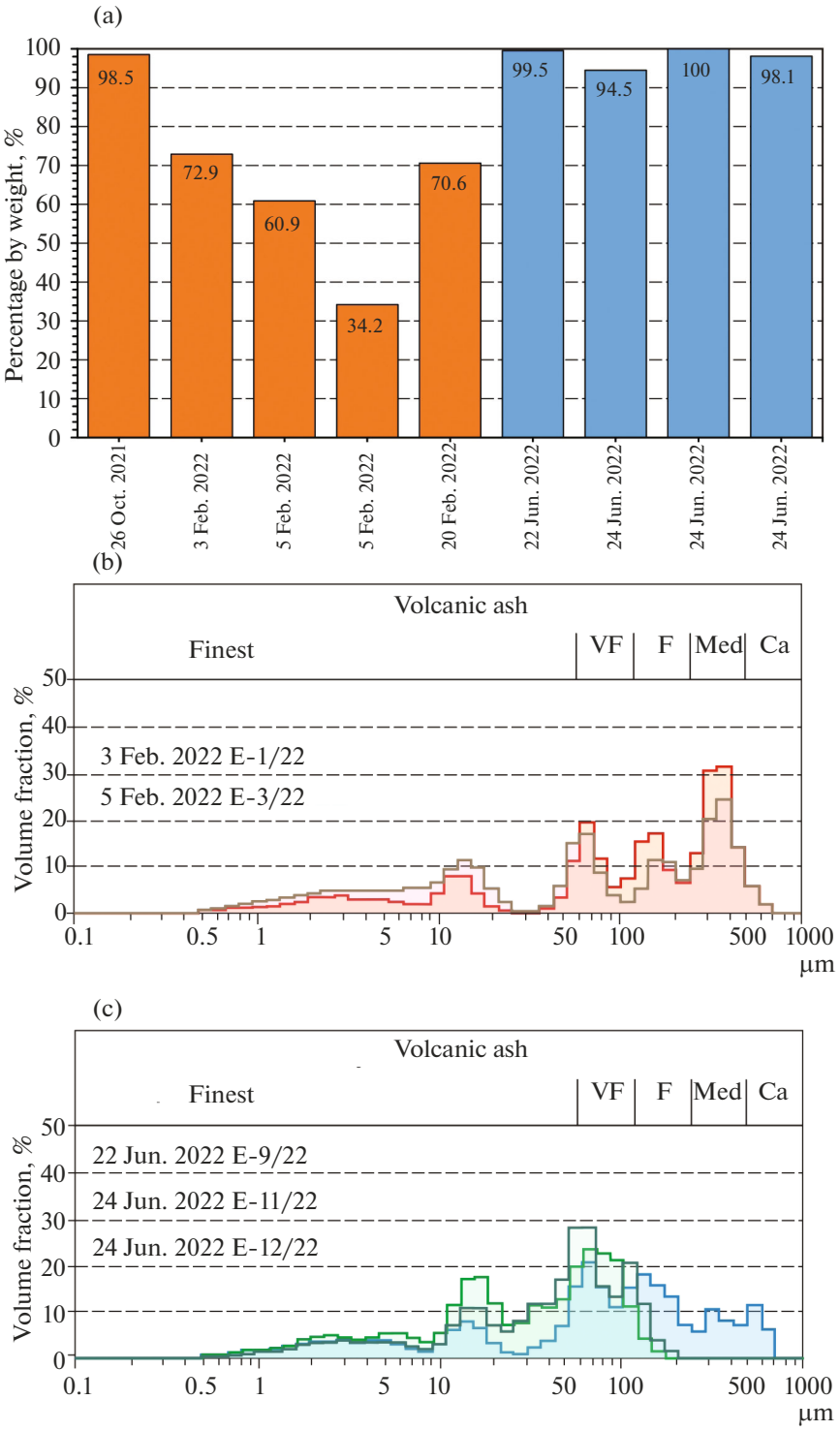

Fig. 6. Particle-size distribution (PSD) of tephra discharged by Ebeko Volcano: (a) weight percentage of the fine fraction (<1 mm) in the late 2021 ash (orange color) and for the ash of the first half of 2022 (blue color); (b) results of laser PSD analysis for the fine fraction of the ash discharged during the first period; (c) results of laser PSD analysis for the ash discharged during the second period. Ash classification based on the size of the fine fraction after (Houghton et al., 2015): Co—coarse, Med—medium, F—fine, VF—very fine.

the fine fractions have a blocky morphology as specified by the classification of Wohletz (1983). Particle shape is nearly isometric or elongate. Gas bubbles are rare and are generally disconnected.

Tephra Mineral and Chemical Composition

The juvenile particles are represented by crystals surrounded by a vitreous groundmass, or vitreous clasts with a homogeneous glass with embedded microlites and phenocrysts of plagioclase (~80%), orthopyroxene and clinopyroxene (~15–20% together), magnetite, and apatite (<5%), which show various degrees of crystal shape perfection (Figs. 7a, 7b). Glass fraction in such particles varies from ~50 to ~10%. Most of the particles consist of crystals and clasts of minerals, with the subordinate amounts of the vitreous particles. Juvenile particles are present in the all studied tephra samples, independently of the eruption period. Visually the holocrystalline particles and those consisting of hydrothermally altered rocks are rare.

Among the fresh homogeneous glass with neutral grey shade in SEM BSE images (*fg*, see Fig. 7), a substance that looks like a glass, but having darker shade in SEM BSE images (hereafter a dark groundmass, *ag*, see Figs. 7c, 7d, 7e) is frequently dispersed. The dark groundmass occasionally was found in a direct contact with fresh glass (see Fig. 7e).

Segregations with dark groundmass in some particles have rounded shapes with crystals apparently directed toward their center (see Fig. 7d). They are frequently separated from the fresh groundmass by a rim of cavities extending along the interface. The outer part of segregations contains small elongated feldspar crystals that are frequently oriented toward the center of the segregation. By composition these crystals correspond to sanidine (see Figs. 7d, 7e).

Plagioclase and pyroxene single crystals are embedded into the segregations, but compositionally they are similar to those outside them. The sanidine of segregations uses plagioclase as a seed. Some of the plagioclase crystals are partially embedded in the fresh glass, while the rest is located in the dark groundmass. Sanidine is completely situated in the dark groundmass of segregations and is not encountered outside them.

The middle of the segregations may contain a cavity or cavities with idiomorphic or xenomorphic crystals of α-cristobalite cut by fissures into polygonal blocks (the 'fish scale' texture) (see Fig. 7d). The volume fraction of the cavities in such segregations is roughly comparable to the volume occupied by crystals and dark groundmass itself (see Fig. 7d).

Particles with completely crystallized groundmass, which frequently contain products of hydrothermal alteration (chlorite, pyrite, and so on) were found in subordinate amounts, while particles comprised of hydrothermal minerals (kaolinite, pyrite, anhydrite, amorphous silica) are scarce (see Fig. 7f).

The ash material ejected by discharges during the both first and second periods compositionally corresponds to andesites with moderate to high potassium contents (Table 1, Figs. 8a, 8b). The bulk composition of this ash is also similar to lavas and volcanic bombs ejected by the Ebeko group volcanoes (Table 2, see Fig. 8) in different periods of their activity. Meanwhile, Fig. 8 demonstrates that the ash bulk compositions are slightly but systematically shifted to higher SiO_2 and lower alkali metal contents. Thus the character of silica and alkali content variations (see Fig. 8, the white arrow) differs from the evolutionary trend for Ebeko group magmas (see Fig. 8, grey arrow). Nevertheless, these lines are intersecting at the field corresponding to the bulk composition of the bombs ejected from the Korbut Crater by the 2021 eruptions.

SEM EDS microanalysis showed that the compositions of fresh glasses in ash particles correspond to high-K trachyrhyolites (Table 3, see Fig. 8). The compositions of groundmass glass of the volcanic bombs were evolving from high potassium trachydacites to trachyrhyolites with a nearly constant total alkali contents (see Fig. 8a). Fresh glasses in ash particles compositionally correspond to the highest-silica groundmass glasses of volcanic bombs. The diagrams in Fig. 8 (a, b, c) demonstrate that Na_2O content decreases, while K_2O increases on increase of SiO_2. The compositions of glass-like substance in the dark groundmass show that it is composed of nearly pure silica with substantial admixtures of alumina and low concentrations of FeO, CaO, Na_2O, and K_2O (Table 4, see Fig. 8). Figure 8 shows that the evolution of its compositions is directed from fresh glass toward depletion in alkalies and enrichment in silica. The same tendency is also exhibited by the concentrations of the other elements (see Table 4).

DISCUSSION OF RESULTS

The 2022 eruption in the Korbut Crater started as comparatively small discharges of material from the bottom of the crater lake. The plumes of these discharges had the 'cock's tail' shape typical of hydrovolcanic eruptions from a bottom of shallow sea or crater lakes (Parfitt and Wilson, 2008; Houghton et al., 2015). Such discharges are formed during the initial phases of both phreatic and phreatomagmatic eruptions at andesitic stratovolcanoes that possess crater lakes, e.g., the 1995–1996 phreatomagmatic eruption of Ruapehu Volcano, New Zealand (Nakagawa et al., 1999) the phreatic eruption of 2007 at the same volcano (Kilgour et al., 2010). Thus, a mere similarity between the morphologies of eruption plumes does not enable reliable identification of eruption type based on this criterion alone. When the KC lake had been completely dried, there was an increase in the frequency of explosions (see Fig. 4) and in their vigor,

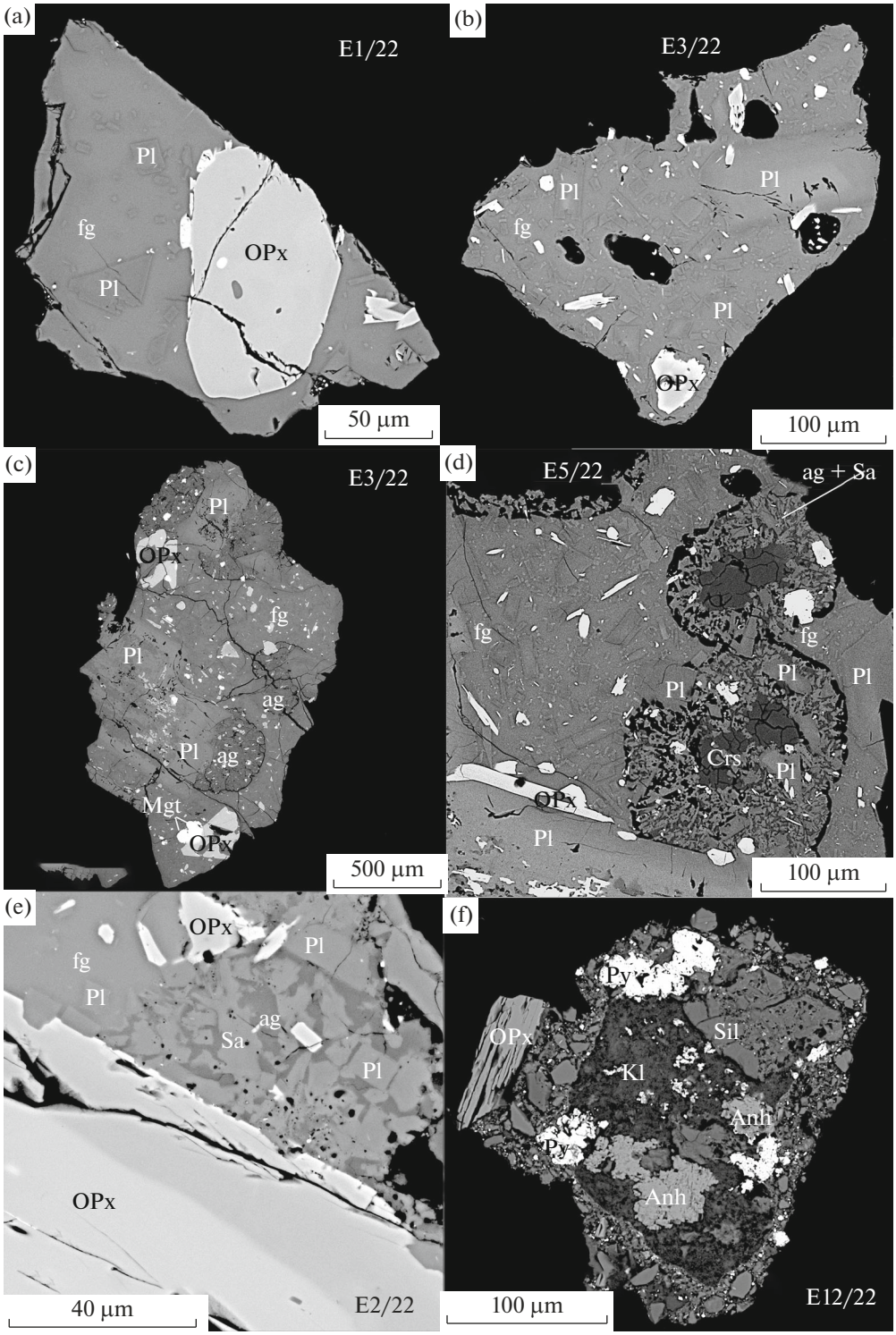

Fig. 7. Particle textures from the fine fraction (<1 mm) of the tephra discharged in 2022. Pl—plagioclase, CPx—clinopyroxene, OPx—orthopyroxene, Sa—sanidine, Crs—cristobalite, Kl—kaolinite, Anh—anhydrite, Py—pyrite, fg—fresh glass, ag—altered glass (dark groundmass). See details in the main text.

accompanied by changes in the morphology of ash plumes. The slight discharges transformed into explosive eruptions of the Vulcanian type. The appearance of breadcrust bombs in the ejecta provided an obvious evidence that juvenile material was involved, and the eruption became a phreatomagmatic one.

Our observations have demonstrated that the discharges from the KC during the first period from Jan-

Table 1. The major-element compositions of the tephra ejected during the eruptions in the Korbut Crater in February-June 2022 (wt %)

Sample no.	E1/2022	E1/22	E2/22	E3/22	E5/22	E11/22	E12/22
SiO_2	55.66	56.05	53.51	54.05	55.72	52.78	54.32
TiO_2	0.67	0.66	0.64	0.65	0.66	0.64	0.62
Al_2O_3	16.52	16.22	16.14	16.24	16.38	16.18	16.16
FeO	8.54	8.65	8.17	8.21	8.19	8.35	8.11
MnO	0.15	0.17	0.13	0.14	0.15	0.13	0.14
MgO	2.96	3.25	2.51	2.83	2.94	2.34	2.73
CaO	6.01	6.27	6.66	6.70	6.47	6.75	6.72
Na_2O	2.66	2.63	2.54	2.62	2.65	2.62	2.65
K_2O	1.94	1.94	1.89	1.89	1.98	1.86	1.91
P_2O_5	0.19	0.17	0.18	0.18	0.17	0.19	0.17
SO_3	0.20	0.21	1.52	1.07	0.56	1.26	0.84
LOI	4.42	3.30	6.08	5.45	3.56	6.17	4.82
Total	99.91	99.51	99.97	100.03	99.43	99.28	99.19

LOI stands for Loss on Ignition. Tephra sampling dates: E1/2022 22 Jan. 2022; E1/22 3 Feb. 2022; E2/22 5 Feb. 2022; E3/22 5 Feb. 2022; E5/22 20 Feb. 2022; E11/22 24 Jun. 2022; E12/22 24 Jun. 2022.

uary to June 2022 brought coarser material whose dominant size was consistent with medium- and coarse-grained ash according to the classification of White and Houghton (2006). When the second period of eruption activity started, from June onward, the PSD has shifted toward finer sizes. We explain this change by different intensities of explosive events. Coarser material discharged during the first period may be largely consisted of particles of lacustrine sediment, which contain, apart from ash, also disrupted large fragments and bombs of previous explosions that fell back into the crater. The low power of the earlier explosions did not result in finer fragmentation of this material. Bearing this in mind, as well as recalling the character and size of the first-period eruption plumes, we believe that these eruptions were related to interaction between lake waters and the vent plug rocks that were supplied with more heat, hence must be classified as phreatic eruptions. Nevertheless, the abundance of juvenile clasts in the ejecta discharged during the first period does not completely exclude the involvement of magmatic material. Since the ongoing eruption activity of the volcano has been lasted for a long time, the juvenile particles could have themselves resulted from fragmentation of both shallow portions of fresh magma and solidified previous portions.

The dominant size of pyroclastic particles discharged during the second period corresponds to very fine and finest ash according to the classification of White and Houghton (2006). According to Wohletz (1983), this provides evidence in favor of the phreatomagmatic mechanism of magma fragmentation. This is fairly well consistent with the increasing vigor of explosions and with the fact that the crater lake had been completely dried before that period.

A study of the chemistry of Ebeko tephra that was ejected in 2022 demonstrated that it corresponds to moderate- to high-K andesites of the calc-alkaline series. They are chemically similar to the volcanic bombs ejected from the KC in 2021 (see Fig. 8) and 2019 pyroclastic material as reported by Belousov et al. (2021). This supports our inference that the tephra was dominantly composed of juvenile material. A small deviation of tephra bulk compositions from the Ebeko magmatic fractionation trend (see Fig. 8) toward enrichment in silica and depletion in other components can be explained both by a mixing with fragmented hydrothermally altered rocks and by the presence of products of interaction between fresh magma and fluids of the volcano's hydrothermal system, which will be discussed below.

The interrelationship of magmatic ejecta discharged during a current eruption activity with previous periods can be drawn from comparison of compositions of fresh glasses between the ejecta. To do this we will compare the compositions of tephra and volcanic bomb groundmass glasses from the 2021–2022 ejecta with the groundmass glass of the volcanic bombs of 1934–1935 eruption. Figure 8 shows that the compositions of the fresh glass in 2022 tephra particles and in the 2021 bomb groundmass are similar. They both are in good agreement with compositions of glasses having the highest silica content in the 1934–1935 bombs. This may probably reflect the compositional evolution of melts during crystallization occurring in the shallow magma chamber that supplies magma to the Ebeko eruptions. This evolution

Table 2. The major-element compositions of the eruption products of Ebeko group volcanoes (wt %)

Sample no.	Pr17-04	Pr17-01	Pr17-02	Pr17-03	Pr17-05	E11/21	E13/21	E14/21	Pr21-12	Pr21-15a	Pr21-16a	Pr21-16b	Pr21-13	Pr21-18	Pr-40*	Pr-60*
Volcano	Ebeko Volcano					Ebeko Volcano										
	Bombs ejected in 1934–1935					Bombs, August 2021			Middle Crater	Southern Crater			Northern Crater			
									Lavas of Holocene eruptions							
SiO_2	55.92	58.28	59.52	56.86	57.68	56.94	56.81	56.81	59.56	59.44	59.81	56.06	54.82	53.29	52.93	53.94
TiO_2	0.68	0.67	0.62	0.68	0.65	0.69	0.68	0.68	0.65	0.64	0.64	0.72	0.72	0.74	0.77	0.73
Al_2O_3	16.90	16.61	16.40	16.89	16.16	16.86	17.00	17.01	15.58	16.10	15.41	16.72	16.98	16.87	17.91	17.72
FeO	9.68	8.28	7.83	9.40	9.35	9.34	9.31	9.18	8.72	8.54	8.80	9.82	9.95	10.82	10.70	10.36
MnO	0.18	0.16	0.15	0.17	0.17	0.18	0.17	0.17	0.16	0.17	0.16	0.18	0.18	0.19	0.19	0.19
MgO	3.10	2.75	2.50	3.13	3.05	3.22	3.17	3.09	2.78	2.69	2.82	3.33	3.59	4.24	4.25	4.00
CaO	7.18	5.92	5.71	7.32	6.66	7.50	7.42	7.39	6.12	6.28	5.84	7.67	8.25	8.51	9.12	8.74
Na_2O	2.89	3.22	3.22	2.91	2.90	2.94	2.98	2.98	3.04	3.01	2.94	2.91	2.79	2.70	2.69	2.76
K_2O	2.10	2.55	2.78	2.08	2.23	2.13	2.10	2.12	2.45	2.46	2.61	1.97	1.92	1.73	1.69	1.75
P_2O_5	0.19	0.12	0.19	0.19	0.17	0.18	0.19	0.19	0.17	0.17	0.16	0.18	0.20	0.21	0.20	0.20
LOI	0.41	0.76	0.33	0.00	0.33	0.00	0.00	0.00	0.38	0.20	0.60	0.14	–0.17	–0.11	–0.14	–0.15
Total	99.24	99.31	99.26	99.64	99.36	99.97	99.84	99.62	99.61	99.69	99.78	99.68	99.23	99.20	100.32	100.24

Sample no.	Pr21-08	Pr21-09	Pr21-10	Pr-30*	Pr-32*	Pr-34l*	Pr-39*	Pr-66A*	Pr21-01	Pr21-02	Pr21-03	Pr21-04	Pr21-06	Pr22-11	Pr22-13	Pr21-11
Volcano	Ebeko Volcano								**	Neza-metnyi	Neozhidannyi			Krasheninnikov		
	pleistocene lavas and dikes								vent	lavas						
SiO_2	59.07	54.90	57.18	58.32	61.35	59.90	60.33	56.46	55.49	54.83	57.98	57.48	56.49	58.61	55.34	58.44
TiO_2	0.61	0.70	0.81	0.60	0.53	0.60	0.57	0.64	0.73	0.68	0.64	0.63	0.65	0.64	0.69	0.63
Al_2O_3	15.63	17.05	16.89	16.56	16.58	16.46	16.77	17.53	16.45	16.99	16.52	16.36	16.90	16.56	17.44	16.69
FeO	8.21	10.48	8.45	8.30	7.30	8.31	7.82	9.58	9.68	10.09	9.10	9.00	9.20	8.64	9.81	8.75
MnO	0.16	0.18	0.14	0.16	0.16	0.16	0.21	0.18	0.18	0.18	0.18	0.17	0.17	0.18	0.18	0.17
MgO	3.66	3.56	2.86	3.70	2.32	2.74	2.54	3.51	3.29	3.71	3.14	3.06	3.23	2.92	3.54	2.96
CaO	6.27	7.30	5.73	6.98	5.59	6.10	5.80	7.37	7.70	7.84	6.71	6.62	7.31	6.63	7.86	6.86
Na_2O	3.02	2.88	3.15	3.08	3.38	3.04	3.36	2.95	2.80	2.75	2.95	2.96	2.92	3.04	2.81	2.94
K_2O	2.40	1.74	2.17	2.19	2.56	2.52	2.47	1.97	1.92	1.80	2.19	2.12	2.03	2.24	1.78	2.27
P_2O_5	0.11	0.23	0.25	0.19	0.18	0.17	0.20	0.18	0.18	0.19	0.19	0.18	0.16	0.18	0.15	0.18
LOI	0.65	0.50	1.64	0.17	0.20	0.00	–0.17	–0.23	0.93	0.10	0.11	0.53	0.14	0.00	0.20	0.07
Total	99.78	99.53	99.28	100.26	100.14	100.01	99.90	100.14	99.34	99.17	99.70	99.12	99.20	99.63	99.80	99.96

* data from (Panin et al., 2015); ** nameless Pleistocene volcano at a distance of 0.5 km northeast of Neozhidannyi. Krasheninnikov Volcano is not part of the Ebeko group, but belongs to the Vernadsky Range.

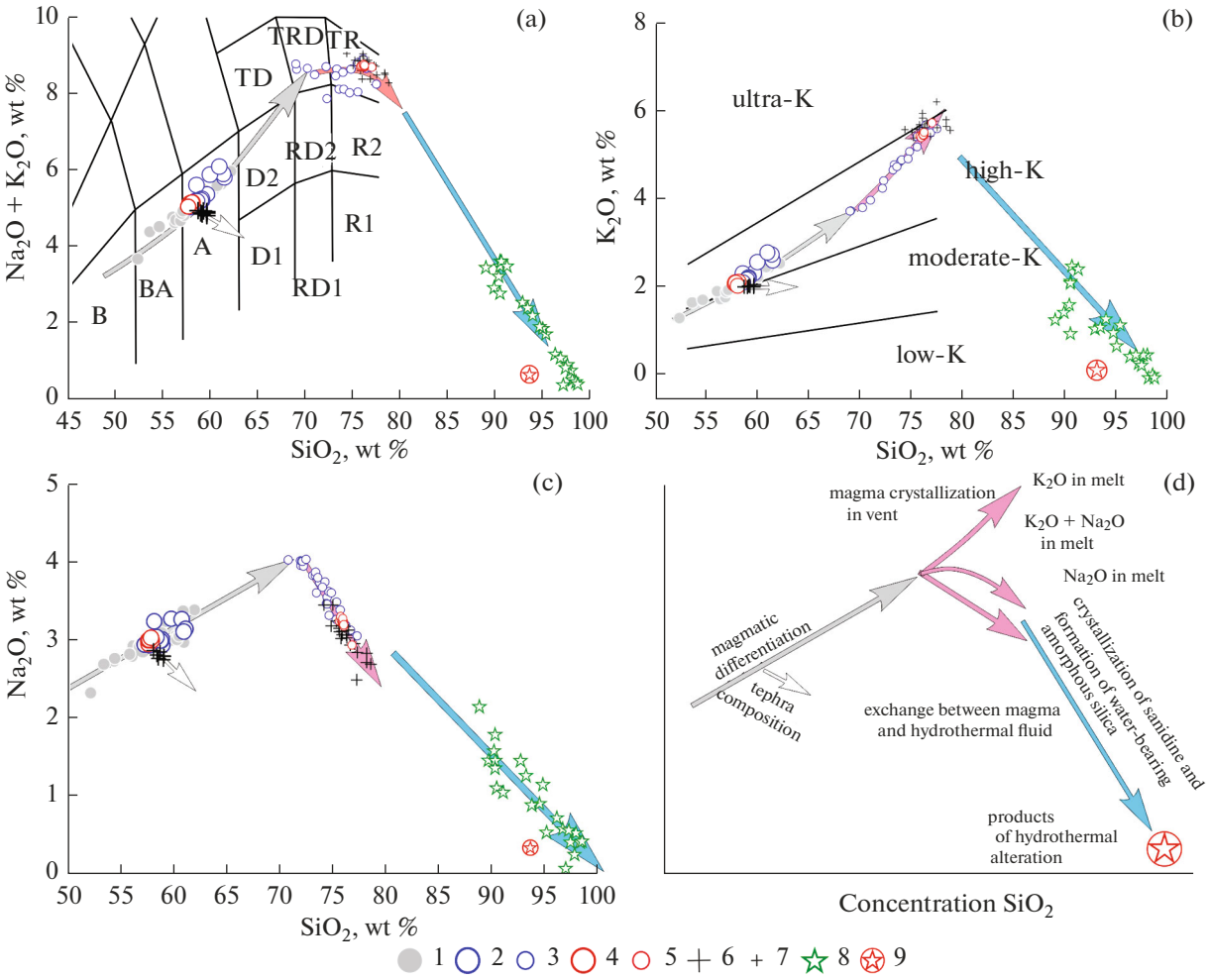

Fig. 8. The compositions of Ebeko Volcano erupted materials. (1) Compositions of lava from the Ebeko group volcanoes (after Panin et al., 2015 and unpublished data of the authors; (2) compositions of the 1934–1935 volcanic bombs; (3) compositions of the groundmass glass of the 1934–1935 volcanic bombs; (4) compositions of the 2021 volcanic bombs; (5) groundmass glass compositions of the 2021 volcanic bombs; (6) bulk compositions of the 2022 tephra; (7) glass compositions of the 2022 tephra; (8) compositions of the vitreous substance of dark groundmass in the 2022 tephra particles; (9) composition of silicic substance in particles of hydrothermal origin (see Fig. 7f). Abbreviations: A andesite, BA basaltic andesite, B basalt, D1 low-alkali dacite, D2 dacite, RD1 low-alkali rhyodacite, RD2 rhyodacite, R1 low-alkali rhyolite, R2 rhyolite, TD trachydacite, TRD trachyrhyodacite, TR trachyrhyolite.

resulted in the enrichment of melts in potassium and depletion in sodium (see Fig. 8d, pink arrows) due to crystallization of plagioclase, clinopyroxene and orthopyroxene with increasing percentage of plagioclase. The latter probably has a decreasing concentration of Ca. The melt of the magma that is involved in the ongoing eruptions has a high-silica trachyrhyolitic composition. This inference is in agreement with the glass compositions of the 2019 pyroclastic material (Belousov et al., 2021). Mass-balanced estimations based on the concentration of K_2O in the glass of the 2021 bombs, indicate that the melt fraction in the magma can be around 40 wt %, which is consistent with visual estimates of glass fraction in the juvenile particles of the 2022 tephra. Such magma must have a high viscosity, poor mobility, and relatively low temperatures.

The compositions of the vitreous substance in the dark groundmass are dramatically different from the fresh glass by their enrichment in silica and depletion in all the other elements. They demonstrate that other processes should operate in the magma along with fractional crystallization of minerals in order to produce the observed changes in melt composition. The intimate relationship between the dark groundmass and the porous and cavernous sections in ash particles implies that these processes might be related to the interaction between the melts and the fluid phase. The insignificant number of gas bubbles in tephra particles and the high totals of microprobe analyses of ash particle glasses tell us that the concentration of magmatic

Table 3. Representative electron probe analyses of fresh glass ejected in tephra from the Korbut Crater in January–June 2022 (wt %)

Sample	E1/22			E3/22				E5/22	
	1	2	3	1	2	3	4	1	2
SiO_2	76.40	73.88	74.86	76.80	77.80	76.13	75.14	75.25	74.38
TiO_2	0.40	0.48	0.47	0.34	0.43	0.48	0.45	0.48	0.49
Al_2O_3	11.72	12.39	11.70	11.55	10.96	11.38	12.68	11.85	12.29
FeO	1.55	2.35	2.03	1.49	1.45	1.68	1.89	2.29	2.29
MgO	0.00	0.10	0.08	0.03	0.00	0.00	0.00	0.25	0.00
CaO	0.23	0.91	0.63	0.72	0.41	0.51	0.78	0.85	0.96
Na_2O	2.48	3.16	3.04	2.84	2.83	2.94	3.25	3.11	3.44
K_2O	6.16	5.48	5.89	5.61	5.64	5.72	5.59	5.47	5.37
Cl	0.08	0.23	0.21	0.14	0.27	0.23	0.15	0.18	0.21
Total	99.01	98.98	98.91	99.50	99.80	99.08	99.93	99.73	99.43
Sample	E5/22			E12/22					
	3	4	5	1	2	3	4	5	6
SiO_2	78.26	77.74	76.76	76.00	75.20	75.87	75.85	75.97	75.06
TiO_2	0.36	0.44	0.42	0.47	0.44	0.37	0.41	0.43	0.44
Al_2O_3	10.78	11.05	12.02	11.81	11.92	11.86	12.37	11.66	11.97
FeO	1.51	1.38	1.95	1.91	2.02	1.95	1.81	1.87	2.01
MgO	0.00	0.00	0.00	0.08	0.12	0.11	0.07	0.07	0.09
CaO	0.44	0.37	0.64	0.62	0.80	0.72	0.94	0.54	0.75
Na_2O	2.70	2.72	2.96	3.03	3.10	3.18	3.25	3.13	3.17
K_2O	5.56	5.79	5.46	5.71	5.48	5.62	5.46	5.70	5.52
Cl	0.20	0.28	0.19	0.22	0.25	0.20	0.22	0.27	0.22
Total	99.81	99.76	100.39	99.87	99.34	99.89	100.38	99.64	99.23

volatiles was low. As well, the gas bubbles generally have a well-pronounced rounded shape and do not contain mineralization, providing evidence of a low concentration of dissolved salts in the magmatic gas and of an absence of reactional interactions between gas and melt. This suggests that the formation of high-silica domains with dark groundmass was due to the interaction of fresh magmatic melt with a fluid that was in a strong disequilibrium with the magma. In our opinion, the fluid in question may either come from the hydrothermal system that is operating beneath and around Ebeko Volcano (Belousov et al., 2002; Rychagov et al., 2004; Kalacheva et al., 2015), or from the seepage from the crater lake.

Round segregations containing sanidine, cristobalite, and dark groundmass frequently show undisturbed crystals of plagioclase and pyroxene, identical with the crystals enclosed in fresh glass (see Fig. 7d). Some of them may be found simultaneously in fresh glass and in dark groundmass. This tells us that the fluid encountered the magma body not through the cracks. Otherwise, the crystals of magmatic minerals would have been split. The round shape of the segregations implies that the original material had the shape of a bubble or a drop that co-existed with the melt. It could have also captured magmatic minerals as it was traveling in the melt.

Sanidine was formed in the studied samples only in the presence of a hypothetical fluid phase, because the original silicate melt contained enough potassium and aluminum. This is rather typical of products of young volcanism and confirm that the silicate material was interacting with aqueous fluids or fumarolic gases at high temperatures (Ganino et al., 2019; Shchipalkina et al., 2020). The groundmass material lost its potassium, aluminum, and partially sodium owing to the crystallization of sanidine (see Fig. 8, the blue arrow). The fluid enclosed in a segregation probably also extracted sodium and other components from the melt, and could contain some amount of silica. This favored the depletion of dark groundmass in all elements except SiO_2 and the formation of cristobalite in the cavities directly from the fluid phase during the latest phases. High-silica composition and a higher

Table 4. Representative electron probe analyses of glass in dark groundmass of tephra particles ejected from the Korbut Crater in January–June 2022 (wt %)

Sample	E2/22	E2/22	E2/22	E3/22	E3/22	E3/22	E5/22	E5/22	E5/22	E5/22	E5/22
	1	2	3	1	2	3	1	2	3	4	5
SiO_2	91.95	90.74	89.62	86.26	98.43	90.54	93.64	97.53	97.98	94.88	93.08
TiO_2	0.20	0.18	0.12	0.12	0.10	0.17	0.27	0.15	0.13	0.12	0.23
Al_2O_3	4.35	5.75	5.71	7.05	1.28	5.39	3.23	1.06	1.28	2.72	3.51
FeO	0.51	0.37	0.28	0.23	0.13	0.26	0.53	0.17	0.23	0.30	0.42
MnO	bdl	bdl	bdl	bdl	bdl	bdl	bdl	bdl	bdl	bdl	bdl
MgO	bdl	bdl	bdl	bdl	bdl	bdl	bdl	bdl	bdl	bdl	bdl
CaO	0.29	0.61	0.41	0.25	0.00	0.22	0.17	0.00	0.00	0.14	0.17
Na_2O	1.13	1.81	1.58	1.42	0.54	1.47	0.53	0.26	0.42	1.16	1.27
K_2O	0.90	1.00	1.64	3.51	0.00	2.18	1.45	0.52	0.52	0.72	1.14
SO_3	bdl	bdl	bdl	bdl	bdl	bdl	bdl	bdl	bdl	bdl	bdl
Cl	bdl	bdl	bdl	0.07	bdl	bdl	bdl	bdl	bdl	bdl	bdl
Total	99.33	100.46	99.34	98.90	100.48	100.22	99.82	99.68	100.57	100.04	99.84
Sample	E5/22	E5/22	E5/22	E5/22	E5/22	E5/22	E5/22	E5/22	E5/22	E5/22	E5/22
	6	7	8	9	10	11	12	13	14	15	16
SiO_2	89.70	95.99	94.79	96.83	94.97	98.88	90.05	98.56	90.55	96.75	94.28
TiO_2	0.25	0.25	0.20	0.18	0.17	0.15	0.13	0.17	0.17	0.12	0.15
Al_2O_3	5.10	2.06	2.85	2.08	3.17	0.89	5.18	0.87	5.39	1.55	3.47
FeO	0.49	0.22	0.33	0.23	0.12	0.13	0.18	0.00	0.49	0.21	0.26
MnO	bdl	bdl	bdl	bdl	bdl	bdl	bdl	bdl	bdl	bdl	bdl
MgO	bdl	bdl	bdl	bdl	bdl	bdl	bdl	bdl	bdl	bdl	bdl
CaO	0.31	0.11	0.18	0.11	0.11	0.00	0.39	0.00	0.27	0.00	0.15
Na_2O	1.36	0.73	1.04	0.08	0.92	0.42	1.11	0.43	1.58	0.57	0.90
K_2O	2.12	0.48	0.98	0.33	1.02	0.07	2.51	0.00	1.90	0.28	1.33
SO_3	bdl	bdl	bdl	bdl	bdl	bdl	bdl	bdl	bdl	bdl	bdl
Cl	bdl	bdl	0.27	0.07	bdl	bdl	bdl	bdl	0.26	bdl	bdl
Total	99.33	99.84	100.65	100.62	100.48	100.54	99.54	100.03	100.61	99.49	100.55

bdl stands for below the detection limits.

(compared with fresh glass) fracturing of the dark groundmass (see Fig. 7e) suggest that the groundmass material originally contained much water and have a consistency like a silica gel.

The cristobalite crystals (see Fig. 7d) that are confined to cavities, and which belong to the low temperature α-modification, are broken up by 'fish scale' fractures and have a habit typical of the rock in felsic extrusive domes (Horwell et al., 2013; Ivanova et al., 2018). Reportedly, such cristobalite grows from the gas phase at temperatures above that of the phase transition from α to β-cristobalite at ~240°C (Horwell et al., 2013).

The obtained data thus suggest that magma is extensively interacted with a fluid in regions where it will be fragmented lately. The certain nature of the fluid is not well constrained yet. However, taking into account the low porosity of vitreous particles and their blocky morphology, we can assert that magma fragmentation was not due to expansion of magmatic gases. A blocky morphology is typical of phreatic and phreatomagmatic fragmentation (Wohletz et al., 2013). The dominantly siliceous compositions of the material that fills the segregations with dark groundmass, sanidine, and cristobalite tells us that the fluid apparently showed an acid reaction (Hedenquist et al., 1994; Lowenstern et al., 2018) and its origin was probably related to the hydrothermal system of Ebeko volcano. The interaction of such a fluid with silicate magmatic substance might favor the formation of segregations that contain water-bearing amorphous silica.

Segregations with a dark groundmass were found only in the ash particles. They have not been detected in the groundmass of volcanic bombs. This suggests that fine fragmentation would be characteristic for those magma domains in the conduit, which contained the products of interaction between the melt and the fluid of the hydrothermal system, probably containing hydrated amorphous silica. Its dehydration in numerous tiny segregations during subsequent heating or magma rejuvenation would favor the development of phreatomagmatic explosions, even when there is no inflow of groundwaters, melt waters, or crater lake waters to the vent. The details and scales of the

implied process have to be studied, and will be a subject of future publications.

CONCLUSIONS

For the first time in the whole history of Ebeko volcano eruptive activity observations, the data on the character of this activity and magmatic ejecta during the terminal phase of a magmatic eruption have been acquired. During a short repose period, the cup-like shape of the crater, high fumarolic discharge in the Korbut Crater, and considerable meteoric precipitation favored accumulation of acid thermal waters above the volcanic vent in the form of a new crater lake. The percolation of lake water along cracks into the vent and the contact of exogenous water with cooling magma led, in turn, to resumption of explosive activity in the form of weak phreatic discharges in January 2022. The morphology and dimensions of the explosion plumes during the first period of activity, the dominance of ash with medium and coarse-grain sizes allowed classification of the explosions as phreatic. Numerous juvenile particles in the tephra ejected during this period could have been both a result of fragmentation of fresh magma and of solidified earlier portions.

Later on, the intensity of phreatic ejections increased and eruption style transformed into Vulcanian type explosions. The character and power of the explosions, decrease in ash particle sizes during the second period (domination by fine and finest ash), the appearance of breadcrust type volcanic bombs, all confirm a phreatomagmatic mechanism of magma fragmentation. Petrographic and mineralogical-geochemical studies of the tephra ejected during both of these periods showed, not only the presence of juvenile material in the tephra, but also an interaction between magma and a fluid, which was probably coming from the hydrothermal system of Ebeko Volcano. This interaction leads to depletion of the magmatic melt in alkali metals and to enrichment in silica. It produced the segregations of amorphous water-bearing silica whose dehydration might also be considered as one of the factors favoring regular resumption of phreatomagmatic explosions.

ACKNOWLEDGMENTS

We thank L.V. Kotenko (Institute of Volcanology and Seismology, Far East Branch, Russian Academy of Sciences) and T.V. Smirnova (Institute of Geology and Mineralogy, Siberian Branch, RAS) for constant participation and active help in sampling work and studies at Ebeko Volcano itself. Great help in microanalytical studies was rendered by the Head of the X-Ray Spectroscopy Laboratory, Institute of Geology and Mineralogy SB RAS, Cand. Sci. (Geol.–Mineral.) N.S. Karmanov. We are grateful to the reviewers for constructive criticism and valuable remarks that have considerably improved this paper.

FUNDING

The volcanological part of this work was performed for research topic no. FWEW-2019-0001 of the Institute of Volcanology and Seismology FEB RAS "Multidisciplinary Study of Large Unique Geothermal Systems, Heat Sources and Metal-Bearing Fluids". The mineralogical, geochemical, and petrographic analyses were supported by the Russian Science Foundation, project no. 20-17-00075.

CONFLICT OF INTEREST

The authors declare that they have no conflicts of interest.

REFERENCES

Alvarado, G.E., Mele, D., Dellino, P., et al., Are the ashes from the latest eruptions (2010–2016) at Turrialba volcano related to phreatic or phreatomagmatic events? *J. Volcanol. Geotherm. Res.,* 2016, vol. 327, pp. 407–415. doi.org/ eores .2016.09.003 https://doi.org/10.1016/j.jvolg

Barberi, F., Bertagnini, A., Landi, P., and Principe, C., A review on phreatic eruptions and their precursors, *J. Volcanol. Geotherm. Res.,* 1992, vol. 52, pp. 231–246. https://doi.org/10.1016/0377-0273(92)90046-G

Basharina, L.A. and Khramova, G.G., The state of Ebeko Volcano in 1966–1967, *Byull. Vulkanol. St.,* 1971, no. 47, pp. 44–51.

Belousov, A., Belousova, M., Auer, A., et al., Mechanism of the historical and the ongoing Vulcanian eruptions of Ebeko volcano, Northern Kuriles, *Bull. Volcanol.*, 2021, vol. 83, no. 4. https://doi.org/10.1007/s00445-020-01426-z

Belousov, V.I., Rychagov, S.N., and Sugrobov, V.M., The North Paramushir Hydrothermal Magmatic System: Geological Structure, Conceptual Model, and Geothermal Reserves, *Vulkanol. Seismol.,* 2002, no. 1, pp. 34–50.

Christenson, B.W., Reyes, A.G., Young, R., et al., Cyclic processes and factors leading to phreatic eruption events: insights from the 25 September 2007 eruption through Ruapehu crater lake, New Zealand, *J. Volcanol. Geotherm. Res.,* 2010, vol. 191, pp. 15–32. doi.org/ eores.2010.01.008 https://doi.org/10.1016/j.jvolg

Fedotov, S.A., Estimates of heat and pyroclastics transport by volcanic eruptions and fumaroles based on the height of their jets and clouds, *Vulkanol. Seismol.,* 1982, no. 4, pp. 3–28.

Ganino, C., Libourel, G., and Bernard, A., Fumarolic incrustations at Kudryavy volcano (Kamchatka) as a guideline for high-temperature (>850°C) extinct hydrothermal systems, *J. Volcanol. Geotherm. Res.,* 2019, vol. 376, pp. 75–85. https://doi.org/10.1016/j.jvolgeores.2019.03.020

Gorshkov, G.S., *Vulkanizm Kuril'skoi ostrovnoi dugi* (The Volcanism of the Kuril Island Arc), Moscow: Nauka, 1967.

Gushchenko, I.I., *Izverzheniya vulkanov Mira. Katalog* (Eruptions of World Volcanoes: A Catalog), Moscow: Nauka, 1979.

Hedenquist, J. W., Aoki, M., and Shinohara, S., Flux of volatiles and ore-forming metals from the magma-hydrothermal system of Satsuma Iwojima volcano, *Geology,* 1994, vol. 22, pp. 585–588.

Hochstein, M.P. and Bromley, C.J., Steam cloud characteristics and heat output of fumaroles, *Geothermics,* 2001, vol. 30, pp. 547–559.

Horwell, C.J., Williamson, B.J., Llewellin, W., et al., The nature and formation of cristobalite at Soufriere Hills volcano, Montserrat: implication for the petrology and stability of silicic lava domes, *Bull. Volcanol.*, 2013, vol. 75, no. 696, pp. 2–19. https://doi.org/10.1007/s00445-013-0696-3

Houghton, B., White, D.L., and Van Eaton, A.R., Phreatomagmatic and related eruption styles, in *Encyclopedia of Volcanoes,* Sigurdsson, H., Ed., Elsevier, 2015, pp. 537–552. https://doi.org/10.1016/B978-0-12-385938-9.00030-4

Ivanova, D.A., Shcherbakov, V.D., Plechov, P.Yu., et al., Cristobalite in extrusive rocks sampled on Bezymianny Volcano, *Nov. Dan. Miner.,* 2018, vol. 52, no. 2, pp. 51–59. https://doi.org/10.25993/FM.2018.52.23628

Kalacheva, E., Taran, Yu., Kotenko, T., et al., Volcano-hydrothermal system of Ebeko volcano, Paramushir, Kuril Islands: Geochemistry and solute fluxes of magmatic chlorine and sulfur, *J. Volcanol. Geotherm. Res.,* 2015, vol. 310, pp. 118–131. https://doi.org/10.1016/j.jvolgeores.2015.11.006

Kilgour, G., Manville, V., Della Pasqua, F., et al., The 25 September 2007 eruption of Mount Ruapehu, New Zealand: Directed ballistics, surtseyan jets, and ice-slurry lahars, *J. Volcanol. Geotherm. Res.,* 2010, vol. 191, pp. 1–14. https://doi.org/10.1016/j.jvolgeores.2009.10.015

Kirsanov, I.T., Serafimova, E.K., Sidorov, S.S., et al., The March-April 1963 eruption of Ebeko Volcano, *Byull. Vulkanol. St.,* 1964, no. 36, pp. 66–72.

Kotenko, T.A. and Kotenko, L.V., A new lake in the Korbut Crater on Ebeko Volcano, Paramushir, Kuril Islands, *Vestnik KRAUNTs, Nauki o Zemle,* 2022, no. 1, iss. 53, pp. 5–11. https://doi.org/10.31431/1816-5524-2022-1-53-5-11

Kotenko, T.A., Kotenko, L.V., Sandimirova, E.I., et al., The eruption of Ebeko Volcano in January–June 2009 (Paramushir Island, Kuril Islands), *Vestnik KRAUNTs, Nauki o Zemle,* 2010, no. 1, issue 15, pp. 56–68.

Kotenko, T.A., Kotenko, L.V., Sandimirova, E.I., et al., The 2010-2011 eruptive activity of Ebeko Volcano, Paramushir Island, *Vestnik KRAUNTs, Nauki o Zemle,* 2012, no. 1, issue 19, pp. 160–167.

Kotenko, T.A., Sandimirova, E.I., and Kotenko, L.V., The 2018 eruptio of Ebeko Volcano, Paramushir Island, in *Materialy XXII regionalnoi nauchnoi konferentsii "Vulkanizm i svyazannye s nim protsessy", posvyashchennoi Dnyu vulkanologa* (Proc. XXII Regional Conference "Volcanism and Related Processes" Devoted to Volcanologist's Day), March 28–29, 2019, Petropavlovsk-Kamchatsky: IViS DVO RAN, 2019, pp. 82–85.

Kotenko, T.A., Melnikov, D.V., and Tarasov, K.V., Gas emission on Ebeko Volcano, Kuril Islands in 2003–2021: Geochemistry, flows, and indicators of activity, *J. Volcanol. Seismol.,* 2022, vol. 16, no. 4, pp. 264–279. https://doi.org/10.31857/S0203030622040058

Kozlov, D.N., *Kraternye ozera Kurilskikh ostrovov* (Crater Lakes on the Kuril Islands), Yuzhno-Sakhalinsk: GBUK "Sakhalinskii Oblastnoi Kraevedcheskii Muzei" IMGiG DVO RAN, 2015.

Lowenstern, J.B., van Hinsberg, V., Berlo, K., et al., Opal-A in glassy pumice, acid alteration, and the 1817 phreatomagmatic eruption at Kawah Ijen (Java), Indonesia, *Frontiers in Earth Science,* 2018, vol. 6, no. 11. https://doi.org/10.3389/feart.2018.00011

Mastin, L.G. and Witter, J.B., The hazards of eruptions through lakes and seawater, *J. Volcanol. Geotherm. Res.,* 2000, vol. 97, pp. 195–214.

Melekestsev, I.V., Dvigalo, V.N., Kiryanov, V.Yu., et al., Ebeko Volcano, Kuril Islands: A history of eruption activity and the future volcanic hazard, Part I, *Vulkanol. Seismol.,* 1993a, no. 3, pp. 69–81.

Melekestsev, I.V., Dvigalo, V.N., Kiryanov, V.Yu., et al., Ebeko Volcano, Kuril Islands: A history of eruption activity and the future volcanic hazard, Part 2, *Vulkanol. Seismol.,* 1993b, no. 4, pp. 24–42.

Melnikov, D.V., Ushakov, S.V., Girina, O.A., and Manevich, A.G., The formation of new lakes in the Active Funnel of Mutnovsky Volcano and in the crater of Raikoke Volcano, in *Materialy XXII Regionalnoi nauchnoi konferentsii "Vulkanizm i svyazannye s nim protsessy", posvyashchennoi Dnyu vulkanologa* (Proc. XXII Regional Conference Volcanism and Associated Processes" devoted to Volcanologist's Day), Ozerov, A.Yu., Ed., Petropavlovsk-Kamchatsky: IViS DVO RAN, 2020, pp. 42–44.

Morrisey, M., Zimanowsky, B., Wohletz, K., and Buettner, R., Phreatomagmatic fragmentation, in *Encyclopedia of Volcanoes,* Sugurdsson, H., Ed., Academic Press, 1999, pp. 431–445.

Nakagawa, M., Wada, K., Thordarson, T., et al., Petrological investigations of the 1995 and 1996 eruptions of Ruapehu volcano, New Zealand: formation of discrete and small magma pockets and their intermittent discharge, *Bull. Volcanol.,* 1999, vol. 61, pp. 15–31.

Nekhoroshev, A.S., Geothermal conditions and heat flow at Ebeko Volcano, Paramushir Island, *Byull. Vulkanol. St.,* 1960, no. 29, pp. 38–46.

Németh, K. and Kósik, S., Review of explosive hydrovolcanism, *Geosciences,* 2020, vol. 10, no. 2, pp. 44. doi.org/ https://doi.org/10.3390/geosciences10020044

Noveishii i sovremennyi vulkanizm na territorii Rossii (Modern and Recent Volcanism in the Area of Russia), Laverov, N.P., Editor-in-Chief, Moscow: Nauka, 2005.

Opyt kompleksnogo issledovaniya raiona sovremennogo i noveishego vulkanizma (na primere khr. Vernadskogo, o. Paramushir) (A Multidisciplinary Study of an Area of Recent and Neotectonic Volcanism: Vernadskii Range, Paramushir Island), *Tr. SakhKNII,* no. 16, Yuzhno-Sakhalinsk, 1966.

Parfitt, E.A. and Wilson, L., *Fundamentals of Physical Volcanology*, Blackwell Publishing, 2008.

Panin, G.L., Gora, M.P., Bortnikova, S.P., and Shevko, E.P., Subsurface structure of the northeastern fumarole field of the Ebeko volcano (Paramushir Island) according to the data of geoelectrical and geochemical studies, 2015,

vol. 9, no. 4, pp. 301–311. doi.org/ *Russ. J. Pac. Geol.,* Pardo, N., Cronin, S.J., Németh, K., et al., Perils in distinguishing phreatic from phreatomagmatic ash; insights into the eruption mechanisms of the 6 August 2012 Mt. Tongariro eruption, New Zealand, *J. Volcanol. Geotherm. Res.,* 2014, vol. 286, pp. 397–414. https://doi.org/10.1016/j.jvolg eores .2014.05.001 https://doi.org/10.1134/S1819714015040077

Rouwet, D., Sandri, L., Marzocchi, W., et al., Recognizing and tracking volcanic hazards related to non-magmatic unrest: a review, *J. Appl. Volcanol.,* 2014, vol. 3, p. 17. https://doi.org/10.1186/s13617-014-0017-3

Rychagov, S.N., Pushkarev, V.G., Belousov, V.I., et al., The Severo-Kurilskoe geothermal field: The geological structure and future uses, *Vulkanol. Seismol.,* 2004, no. 2, pp. 56–72.

Shchipalkina, N.V., Pekov, I.V., Koshlyakova, N.N., et al., Unusual silicate mineralization in fumarolic sublimates of the Tolbachik volcano, Kamchatka, Russia – Part 2: Tectosilicates, *Eur. J. Mineral.,* 2020, vol. 32, pp. 121–136. https://doi.org/10.5194/ejm-32-121-2020

Skripko, K.A., Filkova, E.M., and Khramova, G.G., The state of Ebeko Volcano in the summer of 1965, *Byull. Vulkanol. St.,* 1966, no. 42, pp. 42–55.

Stix, J. and de Moor, J.M., Understanding and forecasting phreatic eruptions driven by magmatic degassing, *Earth Planets Space,* 2018, vol. 70, no. 83. https://doi.org/10.1186/s40623-018-0855-z

Thorarinsson, S., Einarsson, T., Sigvaldason, G., et al., The submarine eruption of the Vestmann Islands 1963–64, *Bull. Volcanol.,* 1964, vol. 27, pp. 435–445.

Walter, T.R., Belousov, A., Belousova, M., et al., The 2019 eruption dynamics and morphology at Ebeko Volcano monitored by unoccupied aircraft systems (UAS) and field stations, *Remote Sens.,* 2020, 12/1961. https://doi.org/10.3390/rs12121961

Waythomas, C.F., Selected crater and small caldera lakes in Alaska: Characteristics and hazards, *Front. Earth Sci.,* 2022, vol. 9. 751216. https://doi.org/10.3389/feart.2021.751216

White, J.D.L. and Houghton, B.F., Primary volcaniclastic rocks, *Geology,* 2006, vol. 34, pp. 677–680. https://doi.org/10.1130/G22346.1

Wohletz, K.H., Mechanisms of hydrovolcanic pyroclast formation: grain-size, scanning electron microscopy, and experimental studies, *J. Volcanol. Geotherm. Res.,* 1983, vol. 17(1–4), pp. 31–63. https://doi.org/10.1016/0377-0273(83)90061-6

Wohletz, K., Zimanowski, B., and Büttner, R., Magma – water interactions, in *Modeling Volcanic Processes. The Physics and Mathematics of Volcanism,* Fagents, S., Gregg, T.K.P., and Lopes, R.M.C., Cambridge: University Press, 2013, pp. 230–257. https://doi.org/10.1017/CBO9781139021562.011

Zimanowski, B., Büttner, R., Dellino, P., et al., Magma–water interaction and phreatomagmatic fragmentation, in *The Encyclopedia of Volcanoes,* Sigurdsson, H., Houghton, B., McNutt, S.R., Eds., London: Academic Press, 2015, pp. 473–484. https://doi.org/10.1016/B978-0-12-385938-9.00026-2

Translated by A. Petrosyan